TD-01-013
Feb. 14, 2001

PROGRESS REPORT ON SUPERCONDUCTING STRAND AND CABLE R&D

E. Barzi, G. Ambrosio, P. Bauer, J.-M. Rey, R. Yamada, A. Zlobin

Abstract:

A summary is given for a majority of the results obtained during year 2000 at Fermilab in the course of the R&D activities on superconducting strands and cables.

1. INTRODUCTION

To build dipole magnets with a nominal field of about 11 T and reliable operation margins, the superconducting material of choice will need the requirements shown in Table I [1], where J_c is the non-copper critical current density in the strand, d_{eff} is the superconductor effective filament diameter, and RRR is the residual resistivity ratio of the copper stabilizer. Within the High Field Magnet (HFM) Project at the Technical Division (TD), two dipole designs are being studied and built, the cosine-theta model and the common coil model.

Parameter	Cos-Theta/ Common Coil
Strand diameter, mm	1.000 / 0.700
J_c(4.2K,12T), A/mm^2	> 3000
d_{eff}, μm	< 40 / 30
Cu, %	45 ± 5
RRR	> 100
Cabling degradation	< 10 %
Bending degradation	- / < 10 %

Table I. Strand requirements for high field magnets.

Nb_3Sn is currently the material most commonly foreseen for the development of high field superconducting magnets, thanks to its high critical temperature, T_{c0}, of 18 K, high upper critical field, B_{c20}, of about 25-28 T (24-25 T at 4.2 K), and commercial availability. As a comparison, the ductile superconducting alloy NbTi has a T_{c0} of 9.5 K and a B_{c20} of 14 T (that reduces to 10-11 T at 4.2 K). Figure 1 compares the critical current density at 4.2 K of Nb_3Sn, NbTi and Nb_3Al as a function of magnetic field. As for Nb_3Sn, Nb_3Al requires high temperature heat treatment in order for the brittle superconducting stoichiometric phase to be formed. The data in Figure 1

refer to Nb/Sn and Nb/Al composites having undergone a one-step heat treatment at 675°C and 750°C respectively [2], [3].

At this time there are three technologies that may reach the J_c goal: Internal Tin (IT) by Intermagnetics General Corporation (IGC), Modified Jelly Roll (MJR) by Oxford Superconducting Technology (OST), and Powder-in-Tube (PIT) by ShapeMetal Innovation (SMI). The former two are based in the US, the latter in the NL. However, experience with industry has shown that the Nb_3Sn purchase volume needed to support the present effort of the DOE National Labs is not sufficient to raise interest in these companies for an aggressive and productive superconductor R&D. This is why the J_c of Nb_3Sn has stationed for the past 4-5 years at the level of 1800-2200 A/mm^2 at 12 T [2]. In the second half of 2000, a 6-month Superconductor R&D National Program for HEP applications of $500,000 was funded by DOE. This program was meant to help industry in providing a higher J_c product. Eventually both main superconductor US companies, OST and IGC, were financed. This program has proved remarkably successful. In only a few months of R&D, both companies improved the J_c of Nb_3Sn by 30%. As a measure of comparison, within the ITER Project from '90 to '96 (the ITER Light project presently includes mainly Japan and Europe), IGC, the only US participating company, received around $ 6 millions for a combination of R&D funding on Nb_3Sn (through DOE SBIR's) and for a 4 ton supply contract from MIT. In the case of ITER, the main R&D objective for the Central Solenoid model, which required 25 tons of Nb_3Sn strand and was successfully tested in Japan last year, was a reduction of AC losses. The other companies that produced wire for this model coil were Mitsubishi, Furukawa, and Vacuum-Schmelze, at a price of about $1000/kg. At this time, Mitsubishi and IGC are manufacturing 26 tons of Nb_3Sn at a rate of 5 tons/year for the Korean Tokamak project K-STAR.

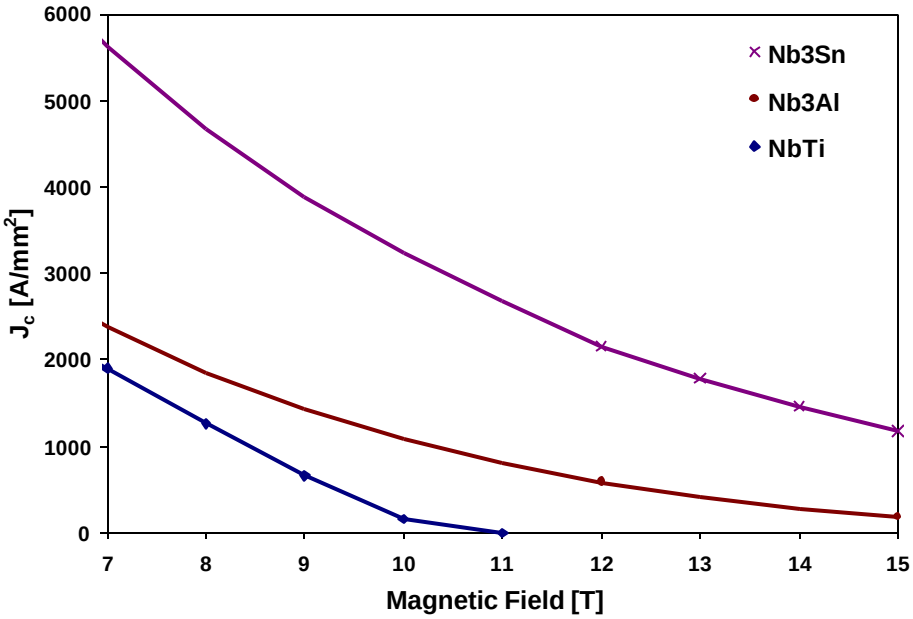

Fig. 1. Critical current density, J_c, at 4.2 K vs. magnetic field for Nb_3Sn, Nb_3Al and NbTi.

At Fermilab, a Short Sample Test Facility (SSTF) [4] to test superconducting strands was commissioned in 1998 at the TD. Probes were designed that allowed routine measurements of critical currents, RRR and magnetization [5]. At the same time, a reaction site with two 36" tube furnaces for operation in argon was set up. This year an optical microscope and a JEOL scanning electron microscope were added to the tools available for superconductor R&D. Thanks to these

tools, Fermilab can perform complete strand characterization and heat treatment optimization, and help companies in their R&D. This note summarizes the results achieved in the past year.

The need of heat treating the Nb/Sn composite to form brittle Nb_3Sn imposes a completely different technology in magnet fabrication with respect to NbTi magnets. At Fermilab, the wind & react approach was chosen for the cos-theta dipole R&D, and the react & wind technique is being explored in the common coil dipole R&D.

2. CRITICAL CURRENT DENSITY

As mentioned above, the J_c required for a 10-11 T accelerator with a safe operating margin is about 3000 A/mm^2 at 12 T and 4.2 K. Figure 2 shows the typical J_c's associated with Nb_3Sn present technologies as a function of field. Shown is also the improvement in J_c achieved by OST and IGC after the 6-month Superconductor R&D National Program, up to 2600 A/mm^2 at 12 T for OST and up to 2400A/mm^2 at 12 T for IGC.

Figure 3 shows the progress in time of the J_c of Nb_3Sn since 1984. A trendline extrapolation suggests achievement of the 3000 A/mm^2 goal within year 2004.

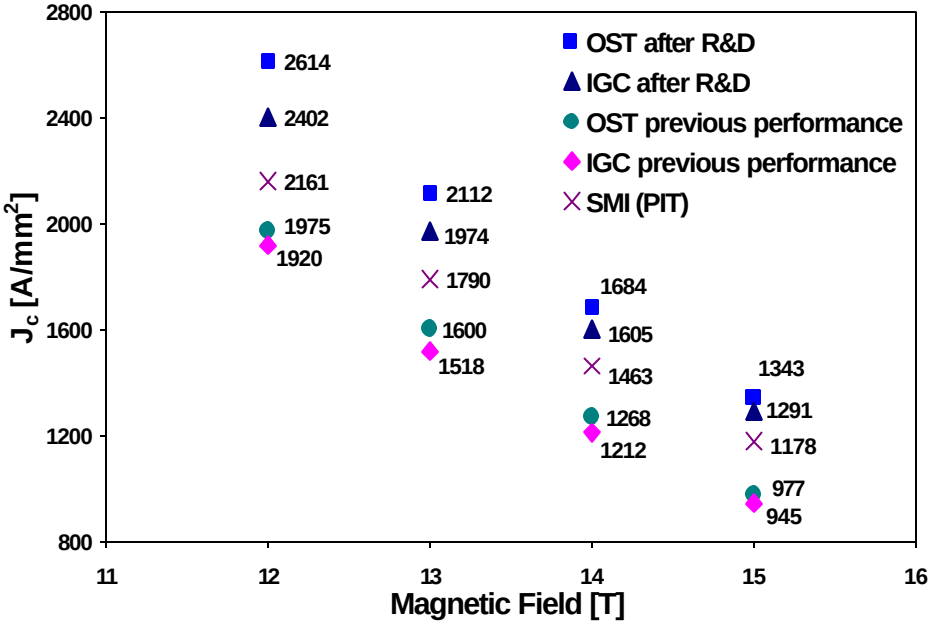

Fig. 2. Improvement in J_c vs. field for Nb_3Sn after the 6-month Superconductor R&D National Program.

The J_c of Nb_3Sn is controlled by a few parameters, like the volumetric fraction of Nb_3Sn that can be packed in the non-Cu part of a strand and the flux pinning mechanism. Strand design optimization is discussed in Section 7 and the importance of flux pinning mechanisms is shown in Section 9. Methods for heat treatment optimization are brought up in Sections 5 and 6.

In magnet design, it is important to know by how much the critical current, I_c, of the original virgin strand gets reduced during magnet fabrication. In the wind & react technique, both strand plastic deformation during cabling (before reaction) [See Section 2.1], and cable compression in the coil during magnet fabrication and operation (after reaction, due to coil precompression and Lorenz force) [See Section 2.3] contribute to I_c degradation. This latter factor is due to J_c sensitivity of Nb_3Sn to strain. In the react & wind method, there is also to take into account the degradation due to the bending strain introduced during winding [See Section 2.2].

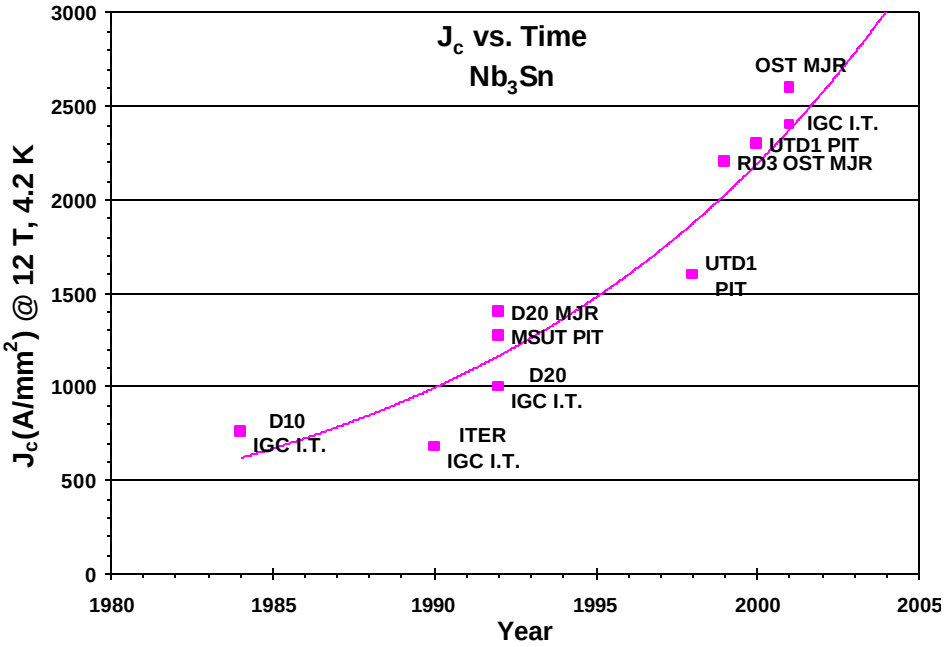

Fig. 3. Improvement in the J_c (4.2 K, 12 T) of Nb_3Sn since 1984 up to date. In Figure, "UT" stands for University of Twente.

2.1 CABLING DEGRADATION

For the development and test of the prototype cable for the cos-theta dipole model, multifilamentary Nb_3Sn strands produced using the MJR (OST), IT (IGC), and PIT (SMI) technologies were used. To optimize the cable geometry with respect to I_c, short samples of Rutherford cable (see Figure 4) with packing factors (PF) in the 85 to 95 % range were fabricated at LBNL and NEEW. The various packing factors were obtained by varying the cable thickness. The results of I_c measurements made on round virgin strands were compared with those made on strands extracted from the cable samples [6]. The cabling degradation was found to increase with magnetic field. Results are shown at 12 T and 4.2 K in Figure 5. In the packing factor range of interest for magnet design (*i.e.* 88-90%), the I_c cabling degradation at 12 T is 7 to 9% for the MJR and IT technologies. Since this study was performed, SMI allegedly produced a new PIT design with a cabling degradation of 5 to 7% only.

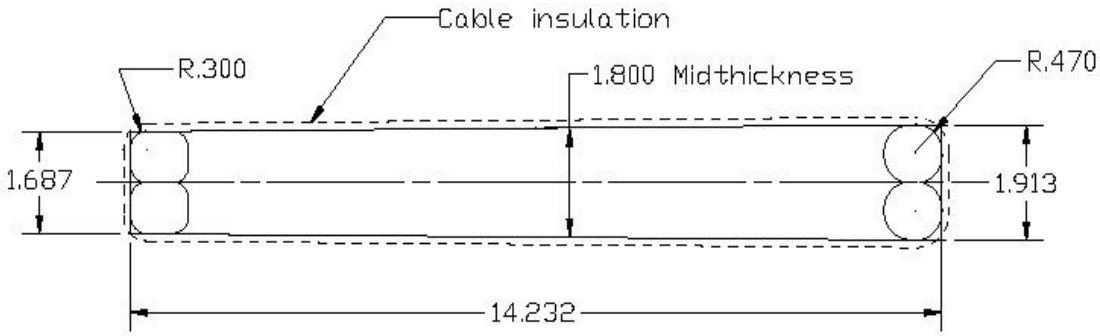

Fig. 4. Rutherford keystoned cable.

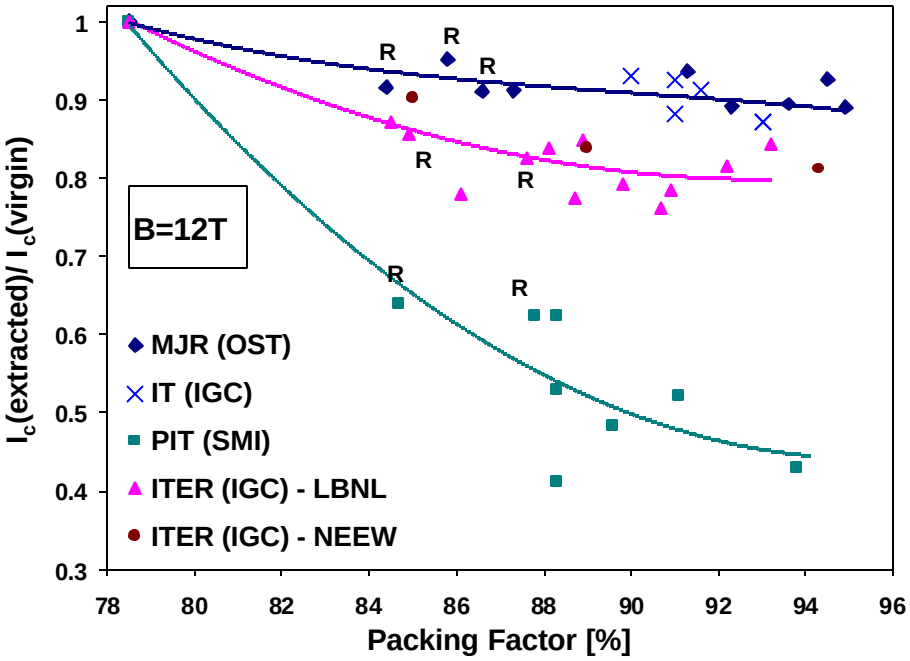

Fig. 5. Critical current degradation due to cabling at 4.2 K and 12 T as a function of packing factor for the IT, MJR and PIT Nb_3Sn technologies [6].

The effective cable J_c at 4.2 K and 12 T normalized to the effective J_c of a cable made of undeformed round strands (PF = 78.5 %) is plotted in Figure 6 as a function of packing factor. For the MJR and IT technologies, the effective J_c has an almost flat behavior with packing factor and is always larger than for round strands. An optimal packing factor range of 88-90% was chosen for the cos-theta model, due to the lower effective J_c and to the mechanical instability of less compacted cables, and to the excessively sharp edges of more compacted ones. Many of these results will be checked in the near future by testing cables made at Fermilab with the recently commissioned cabling machine purchased at IHEP (Protvino, Russia).

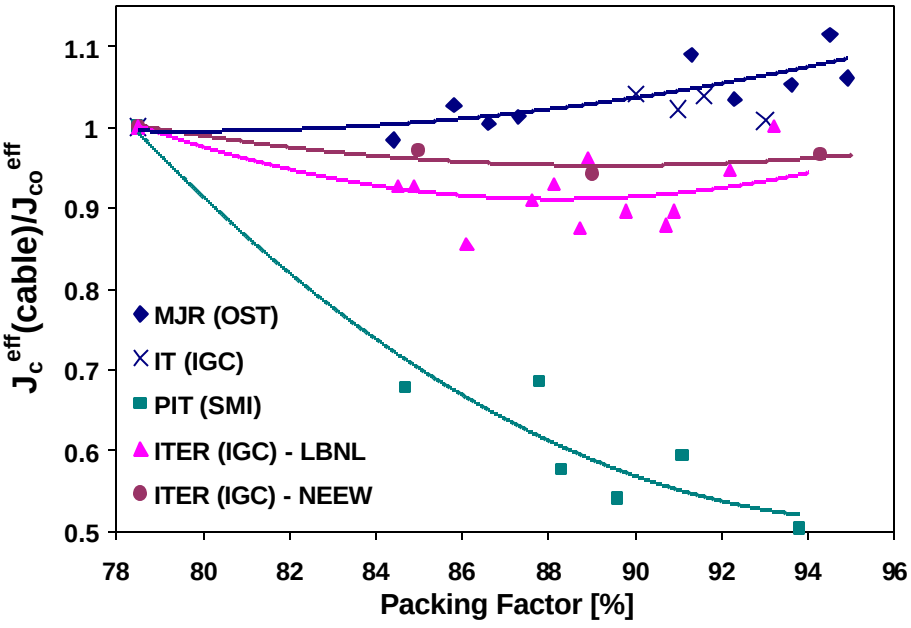

Fig. 6. Effective cable J_c at 4.2 K and 12 T as a function of packing factor for the IT, MJR and PIT Nb_3Sn technologies.

2.2 BENDING DEGRADATION

To measure the critical current degradation due to bending, the sample holders used for reaction have a smaller diameter than those used for measurement, and include a conical part. After reaction, the sample is moved from one holder to the other along the groove of the conical part. This is shown in Figure 7A. The results of I_c measurements made on unbent strands were compared with those made on samples with a maximum bending strain of about 0.2 % and 0.4 % [7]. Figure 7B shows some recent results of bending degradation measured for OST 0.7 mm strands to be used in the first single layer common coil dipole model, which features a minimum bending radius of 90 mm (*i.e.* maximum bending strain of 0.19% for a 0.7 mm wire). For such a magnet, bending degradation at 12 T is therefore expected to be less than 7 %.

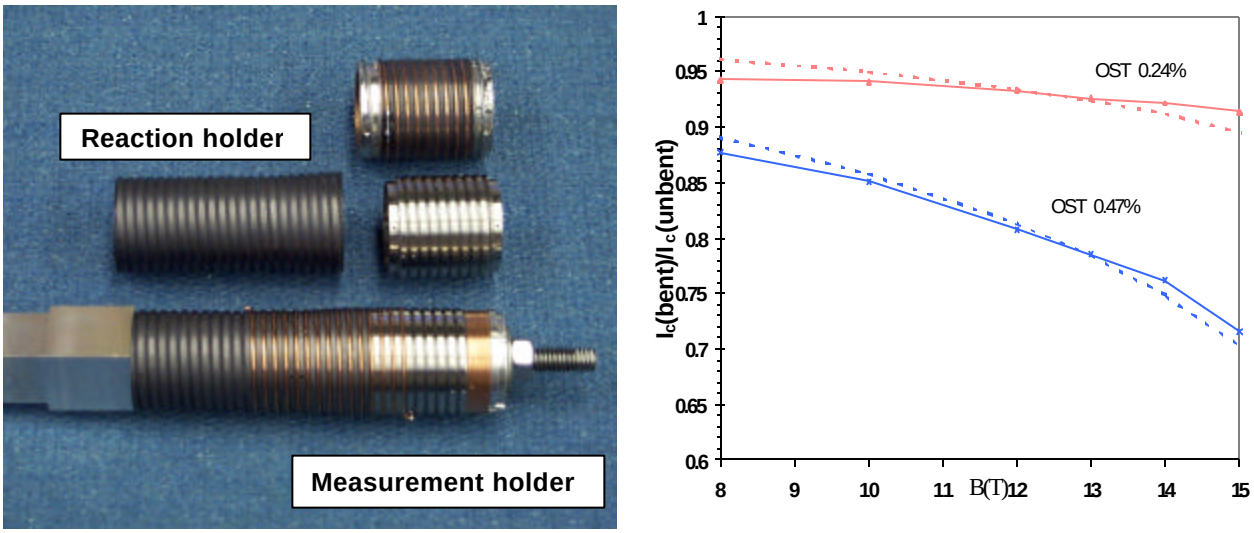

Fig. 7 A. Reaction and measurement samples holders used for bending degradation; **B.** Critical current degradation due to bending strains of 0.2 % and 0.47 % as a function of field for OST 0.7 mm strands to be used in the first single layer common coil dipole model. Dashed lines refer to calculations according to Ekin's strain model [9], assuming an intrinsic strain of 0.1%.

Fig. 8. Cable critical current sample holder before insertion into test station.

Bending degradation was also measured on cables in the cable test facility at NHMFL using the sample holder shown in Figure 8 [7], [8]. The cables were reacted bent on a 290 mm diameter reaction spool, and straightened before impregnation and measurement. Results were compared with those of unbent samples. Figure 9 shows an excellent correlation between strand and cable tests, performed for a Rutherford rectangular cable made with 41 ITER strands 0.7 mm in diameter, in the case of uncored cables whose strand layers bent independently.

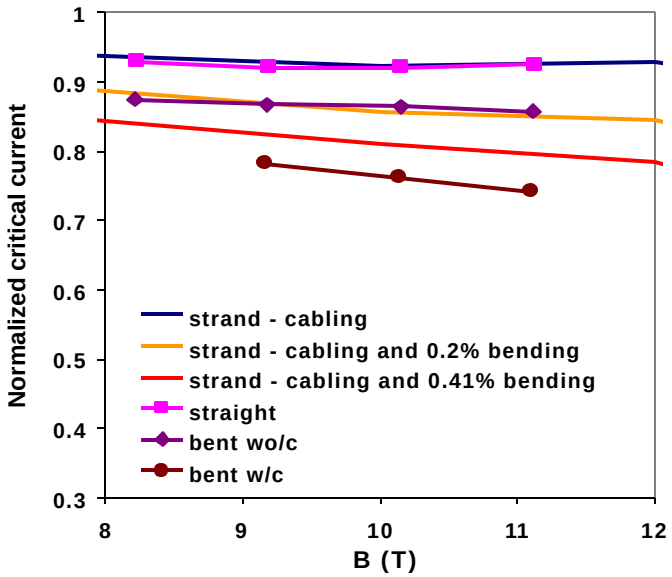

Fig. 9. Critical current normalized to that of 0.7 mm virgin strands as a function of field for a 41-strand ITER cable straight and bent. The lines show results of strand tests [8].

2.3 DEGRADATION UNDER TRANSVERSE PRESSURE

The effect of transverse pressure on the critical current of Nb_3Sn ITER cables was measured in the cable test facility at NHMFL [8]. The cable sample holder is designed to securely hold cable samples in place while applying a transverse stress up to 180 MPa to the cable broad face. Pressure uniformity along the cable sample is ensured by a pressure bar. A cross sectional view of the sample holder is shown in Figure 10A, and results of the transverse pressure effect at various fields for a 41-strand ITER cable are plotted in Figure 10B. In such a case, the critical current appeared to linearly decrease with pressure. At a field of 11 T, the I_c degradation was about 10 % for a pressure of 100 MPa. Results did not depend on the preexistent strain in the material. The labels in Figure 10B indicate the measurement sequence, showing reversibility of the transverse pressure effect.

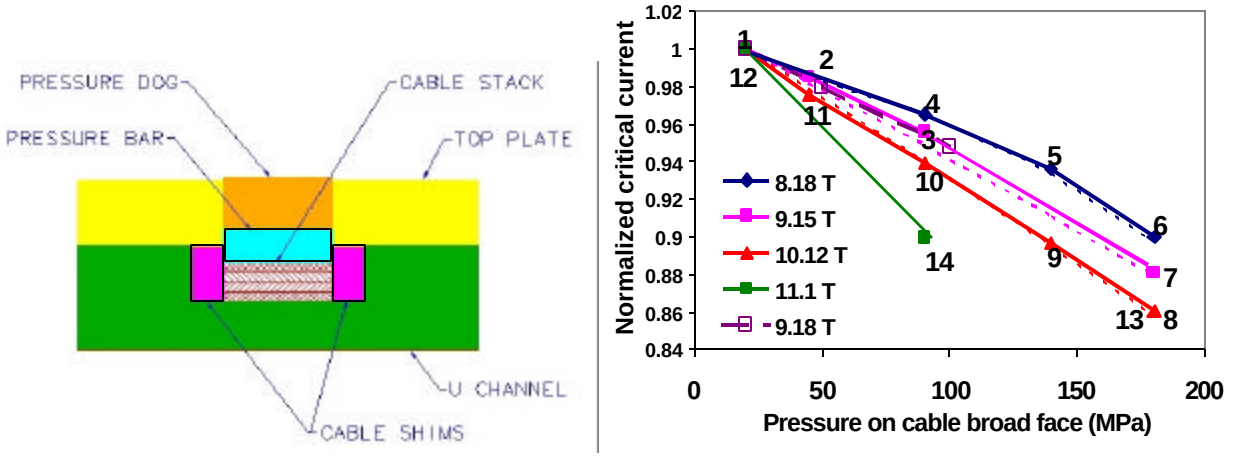

Fig. 10 A. Cross sectional view of cable I_c sample holder; **B.** Effect of transverse pressure on I_c (normalized to its value at 20 MPa) at various fields for a 41-strand ITER cable [8]. Dashed lines were calculated with Ekin's model [9].

Cable tests are a straightforward way to assess magnet performance. However, they are complicated and expensive, especially since the increase in strand J_c requires the use of large cable power supplies. This is why a custom fixture is being built at the TD to assess the superconducting performance of a reacted Nb_3Sn cable under compression by testing the critical current of its *single* Nb_3Sn strand components [10], [11]. This device, called Cable/Strand Strain Test Fixture (C/SSTF), was designed to operate in liquid helium at 4.2 K and in high magnetic fields, and promises to allow considerable time and money savings on cable tests. Its conceptual design is shown in Figure 11A. A cable sample (1) is compressed between two plates (2 and 3). A hydraulic cylinder (4) mounted on the top flange allows applying a pressure up to 200 MPa to the cable sample. The copper leads (5) conveying the current to the sample can carry up to 2000A. Figure 11B shows a view of the final version of the bottom part. Assembly and commissioning of this device are planned for March-April 2001.

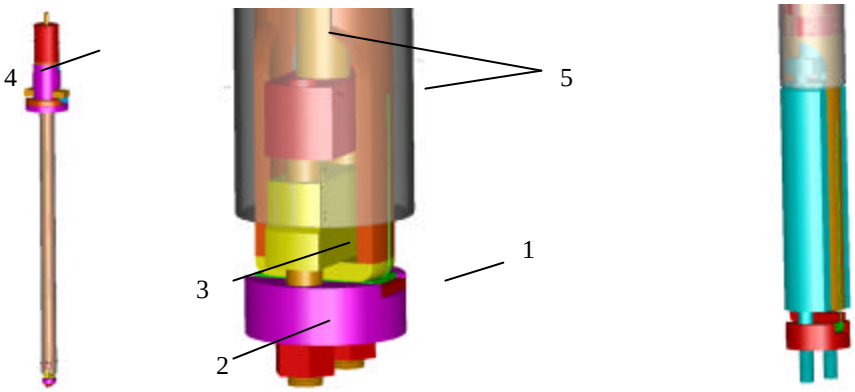

Fig. 11 A. Conceptual design of the Cable/ Strand Strain Test Fixture; **B.** Fixture assembly design after mechanical and thermal analyses.

3. EFFECTIVE FILAMENT DIAMETER

An accelerator magnet also needs excellent field uniformity and magnetic stability. Reference [12] shows that even if the persistent current effect can be reduced with passive corrections, this is possible to the required level only for superconductors with an effective filament diameter, d_{eff}, of less than 30-40μm. The d_{eff} is calculated directly from magnetization loops performed between 10 and 13 T with a balanced coil magnetometer designed at the TD [5], by measuring $\mu_0\Delta M$ and the critical current, I_c, at 12 T (see Figure 12). For present 1 mm high J_c strands, the d_{eff} ranges from about 50 μm for PIT, to 100 μm for MJR [2], and to even larger values for IT. Magnetic instabilities (flux jumps) due to large d_{eff} are assessed by magnetization loops between 0 and 3 T (Figures 13A and 13B).

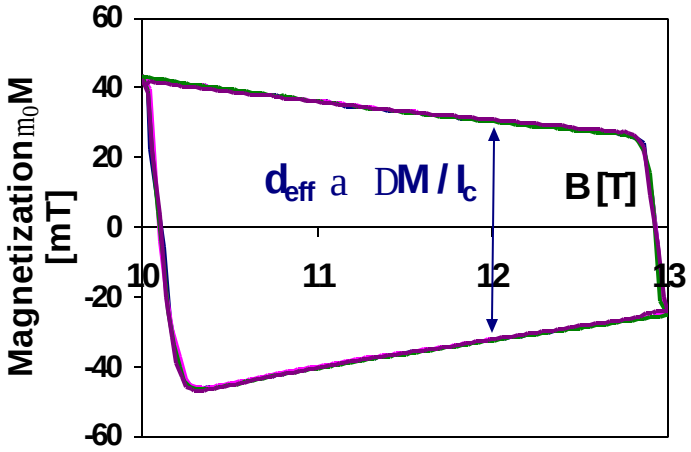

Fig. 12. Magnetization curve per total volume of a Nb_3Sn strand at high field.

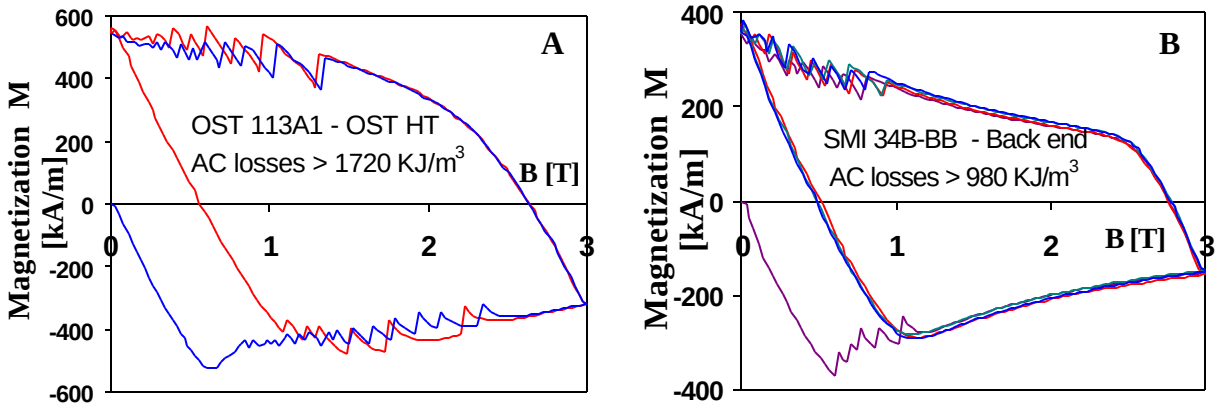

Fig. 13. Magnetization curve per non-Cu volume for a 1 mm MJR strand (**A**) and for a 1 mm PIT strand (**B**). Non-Cu losses are given for 3-0-3 T loops [2].

4. COPPER RRR

The residual resistivity ratio (RRR), defined as the ratio of the Cu resistivity at room temperature over its residual resistivity, is a means to measure strand Cu purity, which is important for strand stabilization and magnet quench protection. Typical values for the present technologies are of about 200 for PIT and IT. For MJR, the RRR depends strongly on the Nb barrier thickness, ranging from about 20, to 60, to 160 for barrier thicknesses of 3, 4.2 and 6 μm respectively (Figure 14).

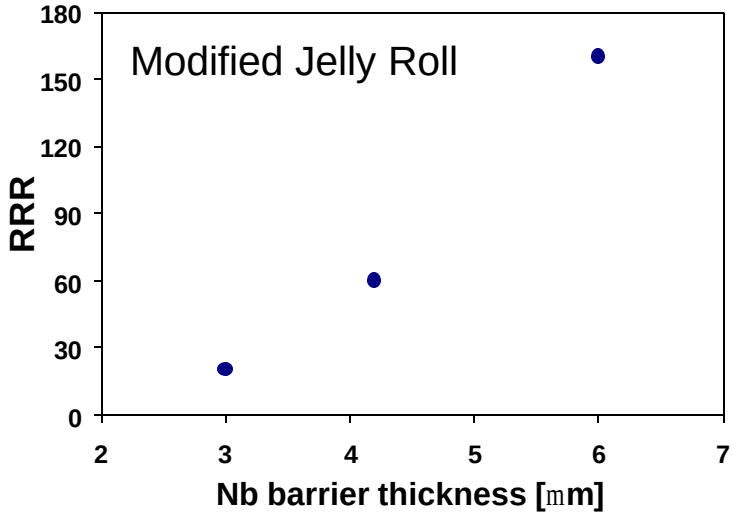

Fig. 14. Variation of RRR with the Nb barrier thickness for Modified Jelly Roll strands by OST.

A low RRR indicates damage of the internal structure of the strand and Sn leakage into the surrounding Cu stabilizer. For instance, Figure 15 shows the case of a MJR strand by OST whose thin Nb barriers did not withstand reaction temperatures for too long, and Sn diffusion contaminated the Cu outside the barriers [2]. Figure 16 shows the effect of cabling on MJR, IT and PIT strands. While in the case of the MJR by OST and the IT by IGC, cabling did not produce significant RRR variations, in the case of the PIT by SMI the RRR fell to less than half its original value. This was attributed to severe dislocation, separation and breakage of the Nb filaments [6].

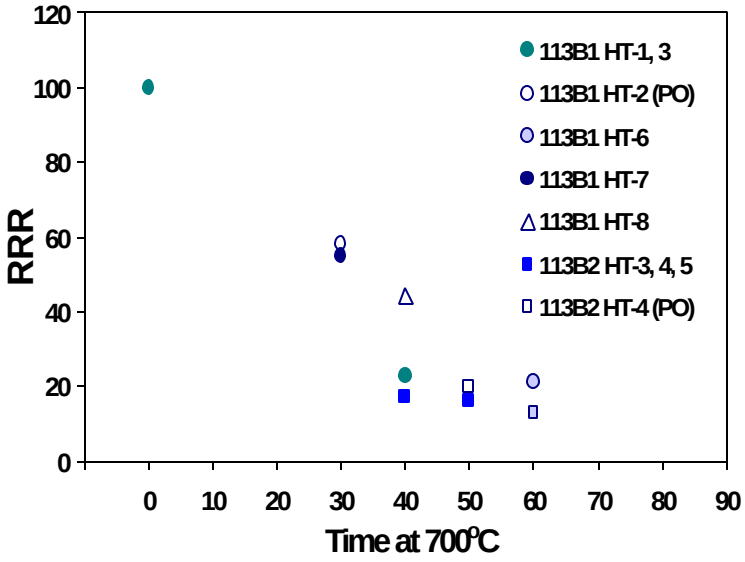

Fig. 15. Variation of RRR with heat treatment time at 700°C [2].

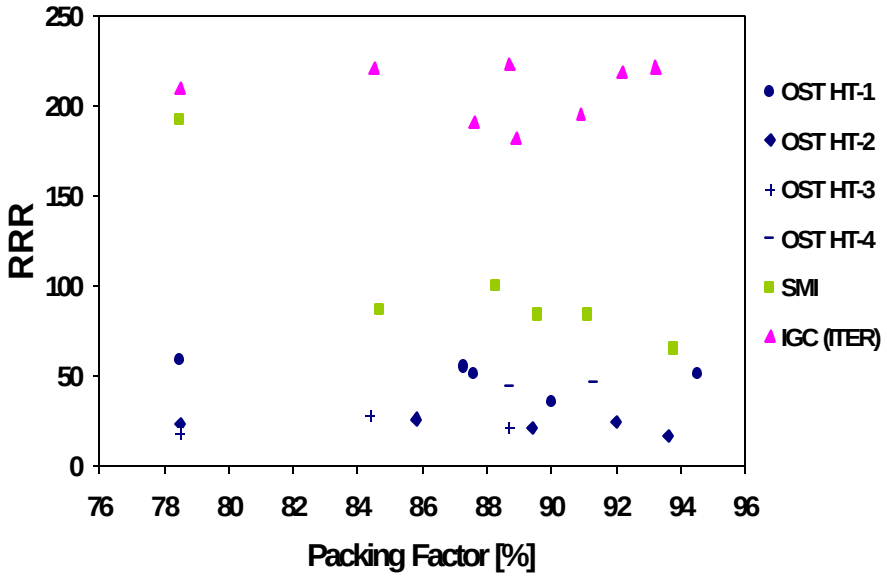

Fig. 16. Effect of cabling on RRR as a function of packing factor [6].

5. REACTION CYCLE

The reaction cycle for Nb_3Sn strands had been optimized at relatively low temperatures (<650°C) due to restrictions imposed by the conductor insulation available until recently. The resulting reaction times for IT and MJR strands were rather long, in the 300 to 600 hour range. Development of high temperature insulating materials allows increasing reaction temperatures, thereby reducing times, without a significant degradation of the strand performance. This would be very important for cost reduction, especially for the wind & react technique. Thanks to numerous optimization studies [13], the duration of the original thermal cycles suggested by the

companies was reduced by a factor of 2 to 4 by increasing the maximum temperature to 700°C (see Figure 17A). However, care must be taken in the removal of some of the low temperature steps unless they can be replaced by a slow overall ramp rate, as in New FNAL-HT in Figure 17A. Otherwise, wire bursts causing tin leakage may occur, as shown in Figure 17B. Another interesting topic that may be related to the heat treatment schedule is strand porosity. At present, all three Nb_3Sn technologies display a large fraction of voids after reaction, as shown in Figures 18A and B for a MJR and a PIT strand. Reducing these voids may increase the J_c and reduce J_c strain sensitivity [14].

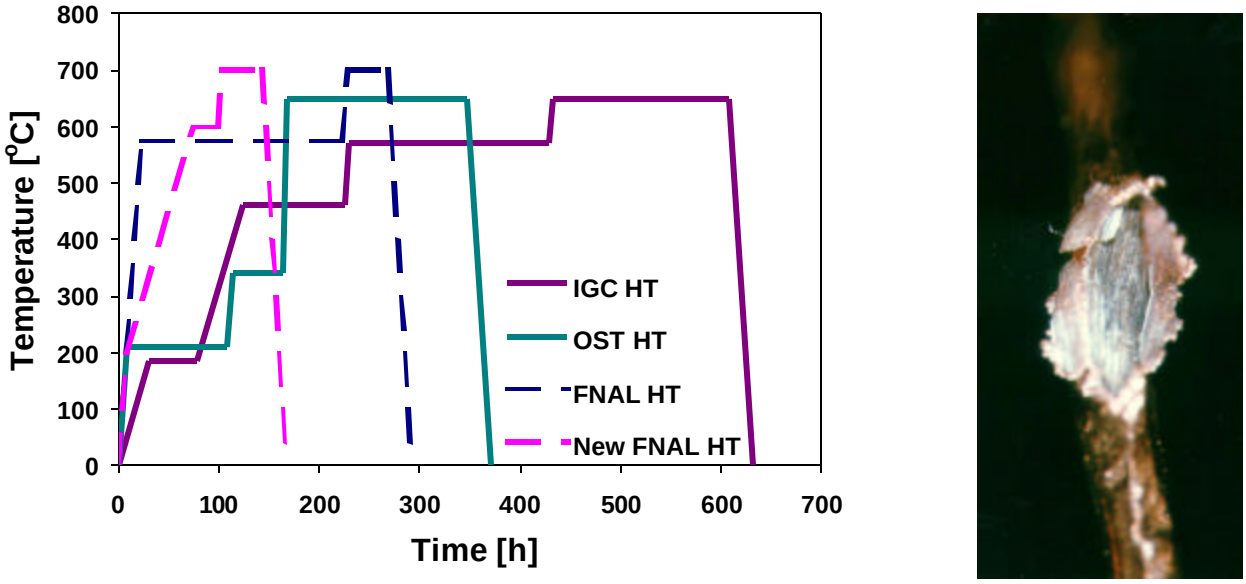

Fig. 17 A. Progressive reduction of heat treatment times; **B.** Copper burst in a Nb_3Sn wire.

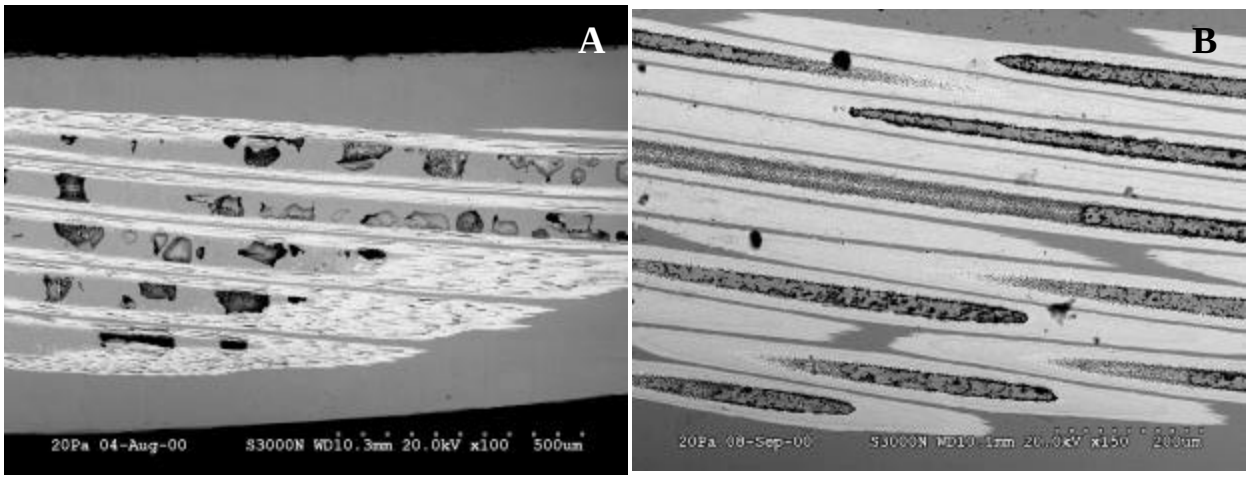

Fig. 18. Large fraction of voids produced after reaction in a MJR (**A**) and in a PIT strand (**B**).

The internal structure of Nb_3Sn, including microstructure and chemical composition, can be better understood with the help of a Scanning Electronic Microscope (SEM) equipped with an Energy Dispersive Spectrometer (EDS). For instance, grain size growth with temperature can be estimated [13], as shown in Figure 19.

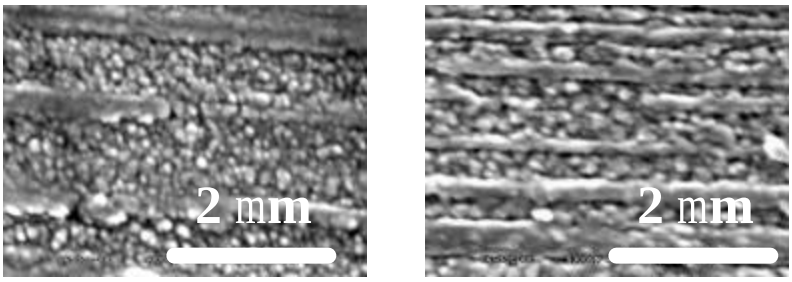

Fig. 19. SEM of longitudinal cross sections of an IT strand after a thermal cycle of 200 hours at 575°C (**A**) and after a cycle including a second step of 50 hours at 700°C (**B**). In case B, the grain size has doubled to about 200 nm from about 100 nm in A [13].

6. Cu-Sn DIFFUSION EXPERIMENTS

During heat treatment of a Nb_3Sn strand, several metallurgical phases are created and eliminated in the course of the Sn diffusion and Nb_3Sn formation processes. Despite Nb_3Sn being since long a well known superconductor, little is known about the kinetics of phase changes. A thorough understanding of the Cu-Sn system diffusion and phase formation processes is necessary to both enhance the superconducting performance and to prevent thermally induced damage of the final conductor. Pure Cu-Sn cylindrical models were designed and fabricated to study formation of the η, ε, δ, γ and β phases of the Cu-Sn phase diagram as a function of time and temperature. By measuring the layer growth of a phase with time and temperature, its diffusion coefficient and activation energy can be calculated.

The effect of phase melting is also important in understanding diffusion phenomena. Figure 20A shows an example of intermetallic compounds formed during a solid state diffusion process at 210°C. Figure 20B illustrates intermetallic compound formation in a solid-liquid diffusion process at 420°C, where the δ phase also developed. This is rarely seen in diffusion experiments made using Nb_3Sn strands, where the presence of Nb perturbs Cu-Sn diffusion [15].

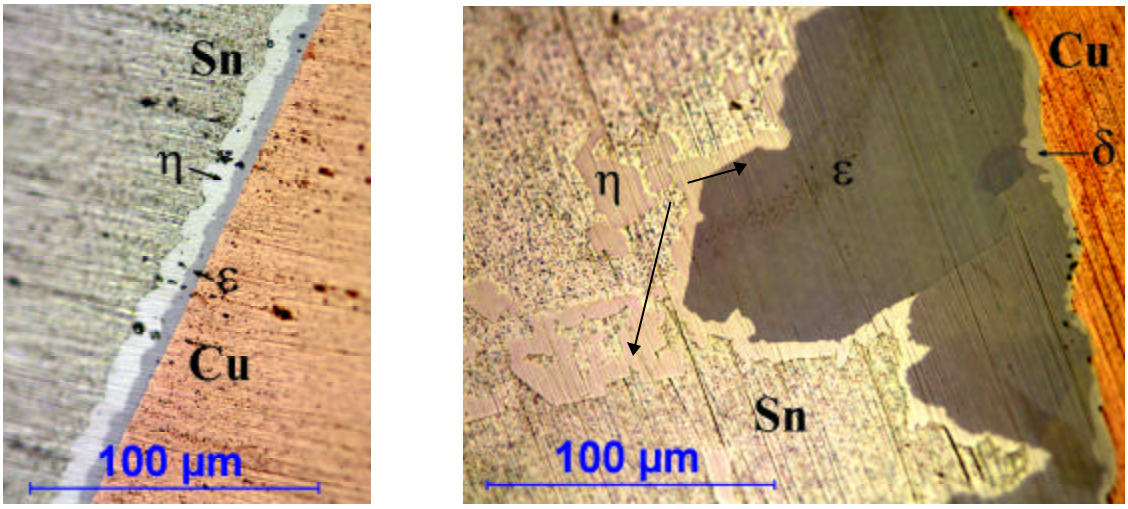

Fig. 20 A. Solid state diffusion process at 210°C for 168 hours: the ε and η phases appear almost simultaneously at the Cu-Sn interface; **B.** Solid-liquid diffusion process at 420°C for 24 hours: first the ε phase appears and grows in the molten Sn, then the δ phase develops through solid diffusion at the ε-Cu interface. The η phase forms only during sample cool down.

7. STRAND DESIGN OPTIMIZATION

For Internal Tin Nb_3Sn, other important fields of study are the effects on J_c of the Nb filament size, the number of strand subelements, and the amount of Sn and of Nb in the non-Cu section.

To better understand the effect of filament size during layer growth, a 575°C reaction cycle that provided only partial reaction of the Nb was applied on the same strand drawn down to different diameters. As can be seen from Figure 21, the reacted Nb_3Sn layer thickness is the same for all strand sizes. It was also found that during layer growth, the J_c dependence on filament size had an exponential behavior for all tested strand designs, as shown at 12 T in the plot of Figure 22. However, after completion of the reaction at 700°C, the J_c at 12 T dropped for a filament size below about 1 μm, as shown in Figure 23 [13].

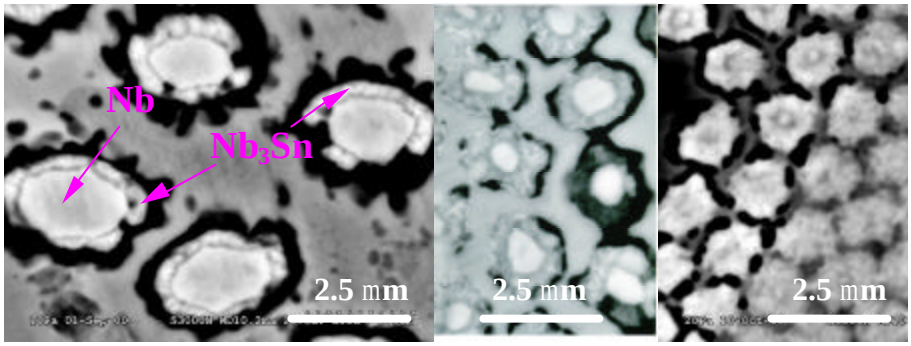

d_{fil} = 2.16 mm **1.30 mm** **0.86 mm**

Fig. 21. Transverse cross section SEM's of an IT strand drawn down to 1.0, 0.6 and 0.4 mm.

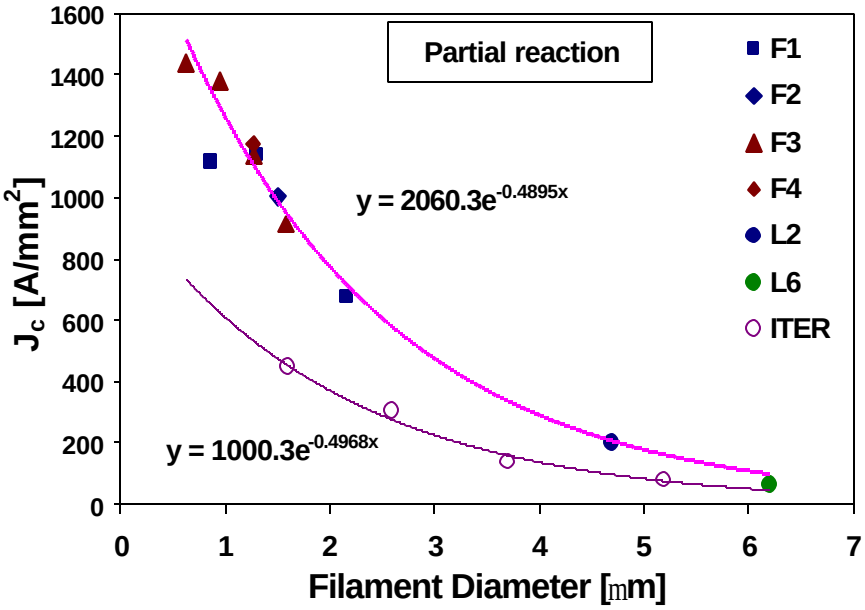

Fig. 22. J_c dependence on filament size at 12 T during layer growth. The symbols in legend represent tested strand designs [13].

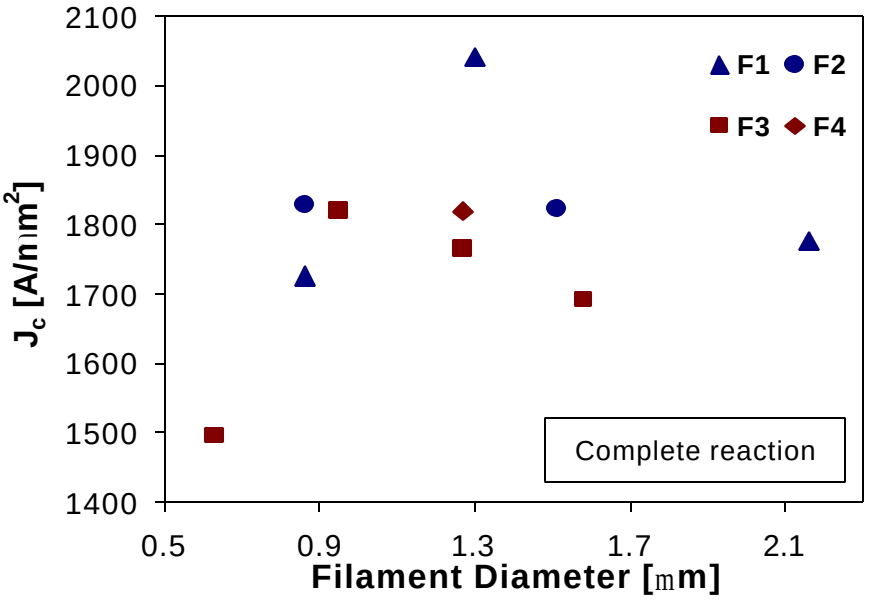

Fig. 23. Peak J_c at 12 T as a function of filament size for fully reacted IT strands. The symbols in legend represent tested strand designs [13].

The number of subelements present in a strand appeared to have an effect in increasing heat treatment efficiency in forming the Nb_3Sn A15 phase. This could be inferred by the different times needed by 19 subelement designs with respect to 37 or 61 subelement designs to reach the peak J_c. Whereas the former required 50 to 70 hours (see Figure 24A), the latter needed only 40 to 50 hours (see Figure 24B) [13].

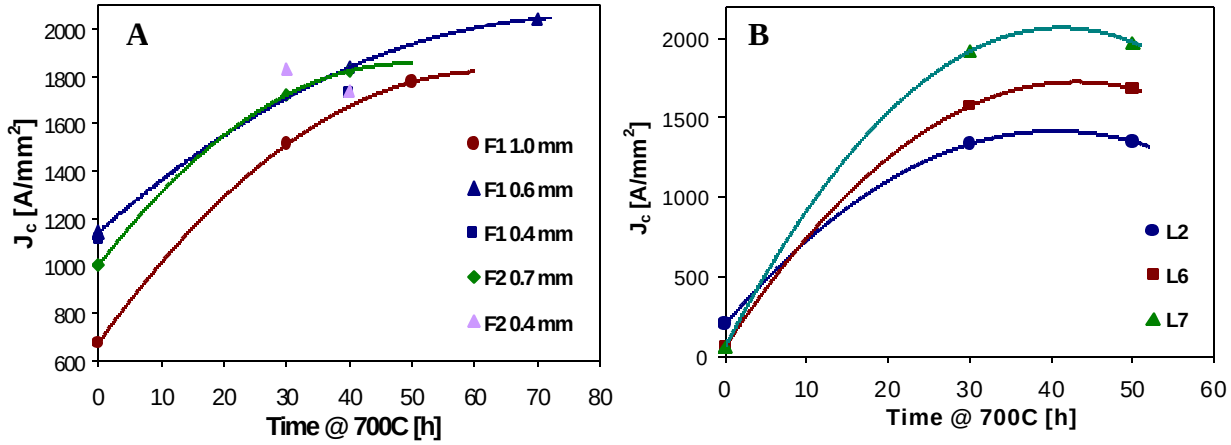

Fig. 24. J_c at 12 T vs. heat treatment time at 700°C for IT strand designs with 19 subelements (**A**) and with either 37 or 61 subelements (**B**) [13].

The J_c of Internal Tin strands appears to be proportional to the atomic percentage of Nb in the non-Cu area of a wire, as clearly shown in Figure 25, where the plotted J_c were produced by different strands having undergone similar thermal cycles. At least two observations can be drawn from this plot. To reach a J_c of 3000 A/mm^2 should require about 50 at.% Nb with the present Internal Tin technology. Also, the maximum achievable intrinsic J_c can be estimated at around 5000 A/mm^2 by extrapolation to 75 at.% Nb in the non-Cu area (*i.e.* the physical limit on Nb content imposed by Nb_3Sn stoichiometry). To improve Nb_3Sn beyond this restriction, action should be taken to modify the flux pinning mechanism in Nb_3Sn, as suggested by the J_c model in Section 9.

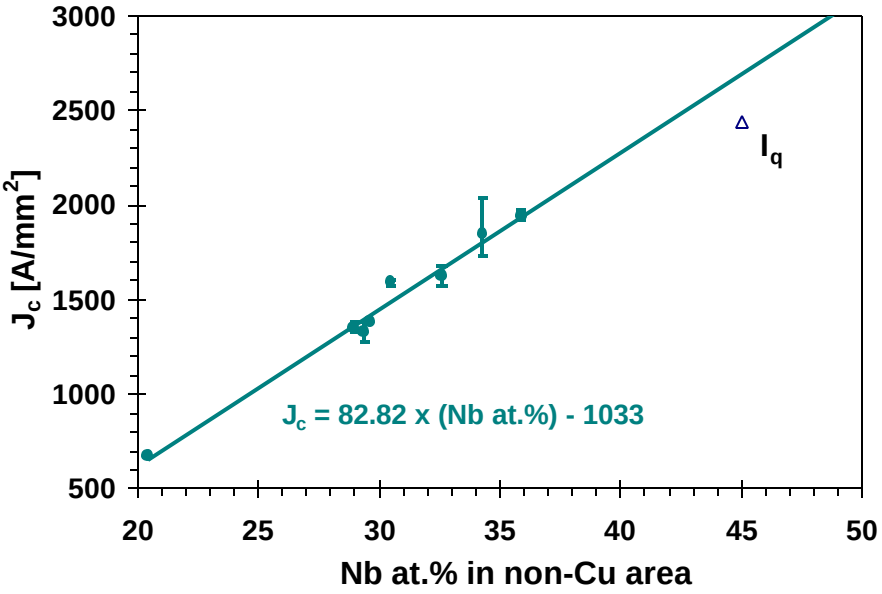

Fig. 25. Critical current density at 12 T as a function of the atomic percentage of Nb in the non-Cu section. The triangle data point represents a quenching current density.

8. Nb_3Sn ANISOTROPIC EXPANSION

It is known that Nb/Sn composite strands expand after reaction due to formation of the Nb_3Sn A15 phase. The value of this expansion is an important parameter for magnet fabrication. Contrary to expectations, the volume expansion during heat treatment observed for the first Nb_3Sn cos-theta models appeared to be anisotropic. Whereas the cable width did not significantly change, the thickness increased by more than expected from volume expansion measurements of round strands. To check that the anisotropic plastic deformation impressed during cabling would release itself during heat treatment [16], a MJR strand was rolled down to two different sizes as a means to apply to it a similar plastic deformation as that due to cabling. A picture of a rolled down strand is shown in Figure 26B. Table II compares dimension measurements before and after reaction. These results confirm the validity of this mechanism. The width expansion is negligible, while thickness expansion is nearly the double of that of a round strand.

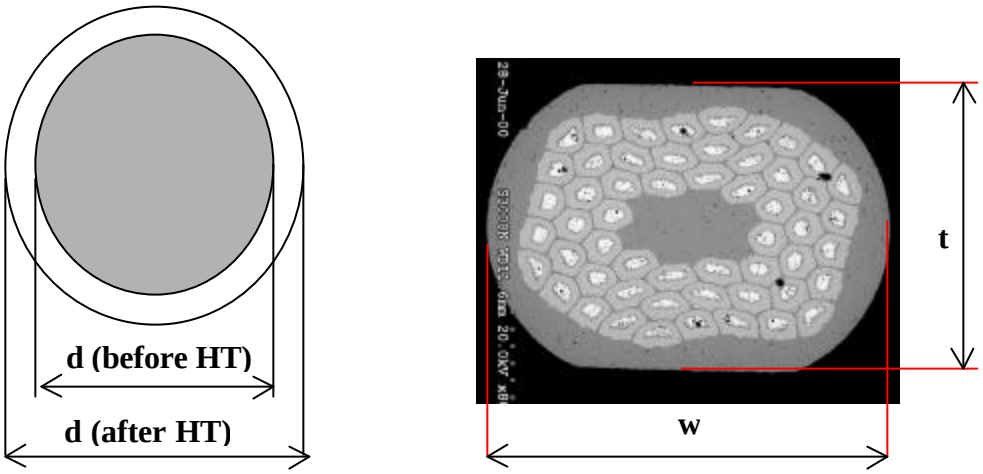

Fig. 26 A. Illustration of the typical isotropic volume increase of a round Nb_3Sn strand after heat treatment; **B.** Result of a similar plastic deformation as that due to cabling that was applied to an OST strand by rolling it down.

Parameter, mm	Before HT	After HT
d	1.001 ± 0.001	1.021 ± 0.001
w_1	1.042 ± 0.004	1.038 ± 0.003
t_1	0.920 ± 0.004	0.955 ± 0.003
w_2	1.064 ± 0.002	1.069 ± 0.003
t_2	0.864 ± 0.005	0.898 ± 0.005

Table II. Dimensions of virgin and deformed MJR strands before and after thermal cycle.

9. A MODEL FOR J_c

A significant progress towards understanding the flux pinning mechanisms in Nb_3Sn was achieved in a recent theoretical model for J_c in granular A15 superconductors by J. McDonald and E. Barzi (MDB) [17]. It is generally agreed that NbTi and Nb_3Sn show very different scaling behavior with respect to flux density and temperature. Many authors have attributed this difference to different mechanisms for flux motion: the scaling behavior of NbTi has been associated with *pin breaking*, while that of Nb_3Sn has been identified with *flux shearing*. In this model, J_c is determined solely by grain boundary pinning. However, this single mechanism can lead to two different scaling laws because of the anisotropy of the pinning forces (see Appendix A). As is apparent from Figure 27B, this model predicts that the J_c at 12 T of Nb_3Sn could be improved by a factor of 4 to 5 by finding a way to increase the *transverse* flux pinning contribution (typical of NbTi) with respect to the *longitudinal* one that prevails in current Nb_3Sn materials.

In Figure 28 are shown some results from using the model (lines) to parameterize recent data (dots) on Nb_3Sn. The agreement is excellent with less than 1% discrepancy over the measured field range. The two technologies encompassed by these data are MJR and PIT.

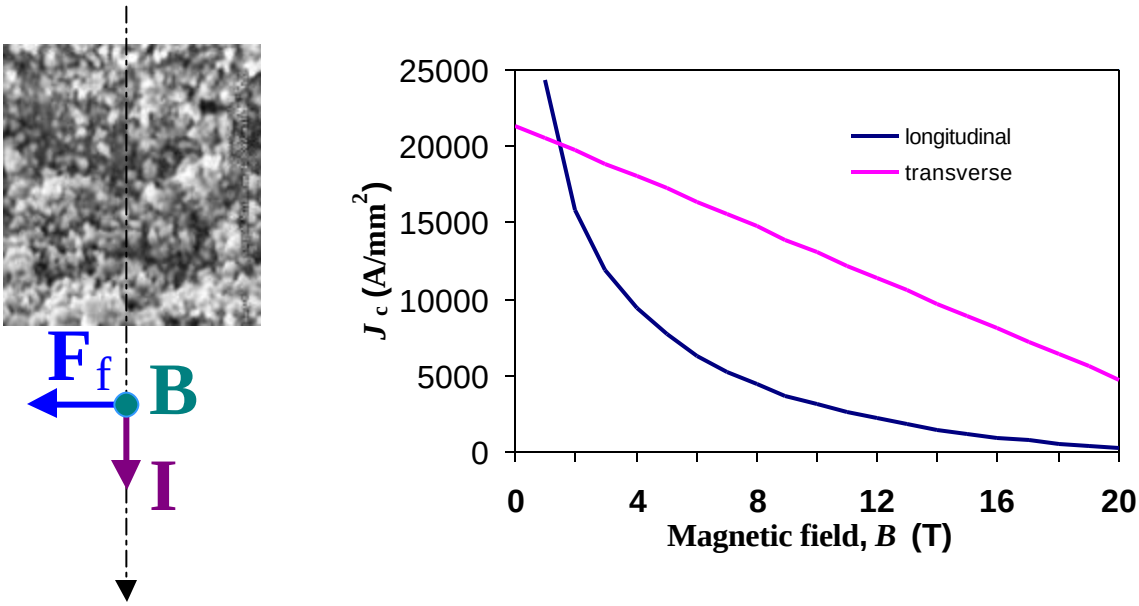

Fig. 27 A. Longitudinal cross section showing equiaxed grains in the middle of a Nb_3Sn reaction layer; F_ϕ represents the force on the fluxons; **B.** J_c vs. magnetic field predicted by the MDB model for *transverse* and *longitudinal* pinning [17]. The model suggests that the J_c at high fields of Nb_3Sn could be improved by a factor of 4 to 5 by finding a way to increase the *transverse* flux pinning contribution.

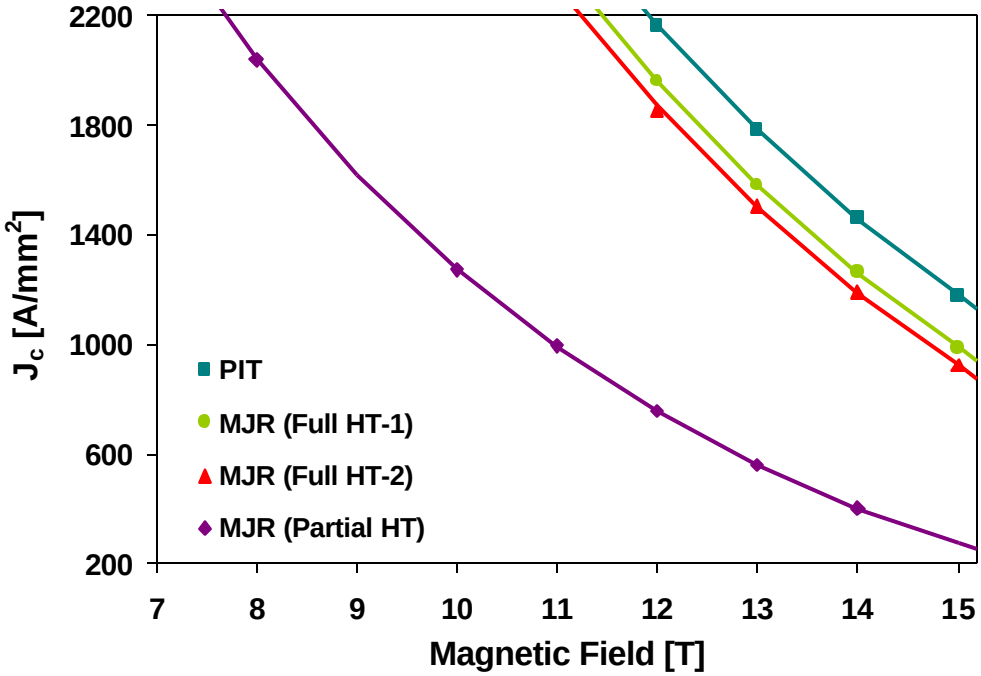

Fig. 28. Application of the MDB model (lines) to parameterize recently measured data (dots) for J_c vs. magnetic field in Nb_3Sn strands [17].

10. CONCLUSIONS

In superconductor R&D, significant progress has been attained at Fermilab in understanding Nb_3Sn strands and cables.

Strand characterization through I_c, magnetization and RRR measurements has allowed thermal cycle optimization. The use of electronic and optical microscopes permits to better study heat treatment effects by visualizing the Nb_3Sn microstructure, and the Cu-Sn diffusion process along its different stages. The impact of the strand design parameters (Nb content, filament size, number of subelements) on the J_c of Internal Tin strands was also better understood and quantified. Finally, a J_c model for A15 conductors that agrees with data with less than 1% discrepancy was realized. This model also suggests that the high field J_c of Nb_3Sn could be improved by a factor of 4 to 5 by increasing the transverse flux pinning contribution with respect to the longitudinal one.

The effect of cabling degradation was measured for all existent Nb_3Sn technologies and for cables to be used in the cos-theta and common coil models. For use in the react & wind technique, bending degradation was evaluated on strands and ITER cables, as was the effect of transverse pressure on ITER cables at NHMFL. A new Cable/Strand Strain Test Fixture to be commissioned soon promises to allow considerable time and money savings on cable tests. It was also found that the Nb_3Sn volume expansion during heat treatment is anisotropic in strands plastically deformed during cabling, due to the release of the cabling plastic deformation.

A 30% improvement in J_c was achieved last year by the US companies OST and IGC after a 6-month Superconductor R&D National Program of $500,000 funded by DOE. It is clear that more funding is needed other than that provided to them by the National Labs R&D for these companies to perform a well structured R&D program on Nb_3Sn.

ACKNOWLEDGMENT

We wish to thank Tom Wokas, whose excellent job made this work possible, and Michela Fratini who tested the majority of the strands of this note.

APPENDIX A

The resulting critical current densities from the MDB model are:

$$J_c^{\perp}(B,T) \approx \frac{B_{c2}}{8\pi\mu_0 \kappa_1^2 D}\left(1-\frac{B}{B_{c2}}\right) \qquad \text{(A1)}$$

in the case of *transverse* pinning, and:

$$J_c^{\parallel}(B,T) \approx \frac{2\alpha d\, B_{c2}^2}{3\sqrt{3\phi_0}\mu_0 \kappa_1^2 D}\left(\frac{\langle J_0 \rangle}{J_d}\right)^2 \frac{\left(1-\frac{B}{B_{c2}}\right)^2}{\sqrt{B}} \qquad \text{(A2)}$$

in the case of *longitudinal* pinning, where:

D is the average grain size,
$k_1 = B_{c2}/2^{1/2}B_c$,
$m_0 = 4\pi$ x 10^{-7} Wb/(A m) is the permeability of free space,
J_0 is the maximum Josephson current density of the Josephson-coupled grain array,
$a = dJ_0/<J_0>$ is the ratio of the decrement in J_0, dJ_0, to the average value, $<J_0>$,
J_d is the depairing current density of the grains,
d is the effective size of the pinning site (~ the grain boundary thickness), and
$f_o = 2$ x 10^{-15} Wb is the quantum of magnetic flux.

The temperature dependence is determined by $B_{c2}(T)$ and $\kappa_1(T)$, and possibly by $\langle J_0 \rangle / J_d$ if the boundaries are metallic.

REFERENCES

[1] G. Ambrosio, E. Barzi, P. Bauer, V. Kashikhin, G. Sabbi, R. Yamada, A.V. Zlobin, "Superconductor Requirements for the HFM Program at Fermilab", FNAL TD-99-073, Dec. 15, 1999.

[2] E. Barzi et al., "Study of Nb_3Sn Strands for Fermilab's High Field Dipole Models", ASC, Virginia Beach, VA, Sept. 17-22, 2000.

[3] E. Barzi, "Sumitomo's Nb_3Al J_c Measurements at the SSTF", FNAL TD-99-004, Jan. 25, 1999.

[4] E. Barzi et al., "Short Sample J_c Measurements at the Short Sample Test Facility", TD-98-057, Oct. 13, 1998.

[5] C. Boffo and E. Barzi, "Magnetization Measurements at the SSTF", FNAL TD-99-036, 1999.

[6] E. Barzi et al., “Strand Critical Current Degradation in Nb_3Sn Rutherford Cables”, ASC, Virginia Beach, VA, Sept. 17-22, 2000.
[7] G. Ambrosio et al., “Study of the react and Wind Technique for a Nb_3Sn Common Coil Dipole”, IEEE Trans. on Appl. Superconductivity, V. 10, No 1, March 2000.
[8] P. Bauer et al., “Fabrication and Testing of Rutherford-type Cables for React and Wind Accelerator Magnets”, ASC, Virginia Beach, VA, Sept. 17-22, 2000.
[9] J. W. Ekin, “Strain scaling law and prediction of uniaxial and bending strain effects in multifilamentary superconductors”, Filamentary A15 Superconductors, M. Suenaga and A. F. Clark, Editors, New York, Plenum Press, 1980.
[10] E. Barzi and A. Zlobin, “Conceptual Design of a Device to Test a Strand in an Impregnated Cable under Compression”, TD-00-032, Apr. 15, ’00.
[11] M. Fratini and E. Barzi, “Mechanical and Thermal Analysis of the Cable/Strand Strain Test Fixture”, Fermilab, TD-01-001, Oct. 31, ‘00.
[12] V.V. Kashikhin and A.V. Zlobin, “Correction of the Persistent Current Effect in Nb_3Sn Dipole Magnets”, ASC, Virginia Beach, VA, Sept. 17-22, 2000.
[13] E. Barzi et al., “Heat Treatment Optimization of Internal Tin Nb_3Sn”, ASC, Virginia Beach, VA, Sept. 17-22, 2000.
[14] D. R. Dietderich et al., “Critical Current of Superconducting Rutherford Cable in High Magnetic Fields with Transverse Pressure”, IEEE Trans. on Appl. Superconductivity, V. 9, pp. 122-125, 1999.
[15] M. T. Naus, P. J. Lee and D. Larbalestier, “The Influence of the Starting Cu-Sn Phase on the Superconducting Properties of Subsequently Reacted Internal-Sn Nb_3Sn Conductors”, ASC, Virginia Beach, VA, Sept. 17-22, 2000.
[16] N. Andreev, Private communication.
[17] J. McDonald and E. Barzi, “A Model for J_c in Granular A-15 Superconductors”, ASC, Virginia Beach, VA, Sept. 17-22, 2000.